LA-8111

A 4 K to 20 K Rotational-Cooling Magnetic Refrigerator Capable of 1-mW to >1-W Operation

University of California

LOS ALAMOS SCIENTIFIC LABORATORY
Post Office Box 1663 Los Alamos, New Mexico 87545

A 4 K TO 20 K ROTATIONAL-COOLING MAGNETIC REFRIGERATOR CAPABLE OF 1-mW TO >1-W OPERATION

by

J. A. Barclay

ABSTRACT

The low-temperature, magnetic entropy of certain single-crystal paramagnetic materials, such as $DyPO_4$, changes dramatically as the crystal rotates in a magnetic field. A new magnetic refrigerator design based on the anisotropic nature of such materials is presented. The key advantages of the rotational-cooling concept are (1) a single, rotary motion is required, (2) magnetic field shaping is not a problem because the entire working material is in a constant field, and (3) the refrigerator can be smaller than comparable magnetic refrigerators because the working material is entirely inside the magnet at all times. The main disadvantage of the rotational-cooling concept is that small-dimension single crystals are required.

I. INTRODUCTION

Jeffries[1] and Abragam[2] suggested in 1963 that nuclei could be polarized simply by rotating a suitable crystal in a magnetic field at low temperatures. The proposed technique involves cyclically transferring a large paramagnetic-ion polarization to nuclear spins without the use of microwaves and with no constraint on the uniformity of the magnetic field. It requires a very anisotropic g-factor for the paramagnetic ion. The rotational-cooling method has successfully produced polarized proton targets.[3]

In the magnetic refrigerator to be described here, the temperature changes associated with changes in the large paramagnetic-ion polarization are used directly to heat or cool a heat-exchange fluid.

II. MAGNETIC REFRIGERATION DESIGN

A. Principle of Operation

The material chosen to illustrate the design is $DyPO_4$, a readily available, stable compound, the magnetic and thermal properties of which have been studied previously.[4,5] $DyPO_4$ has the tetragonal zircon-($ZrSiO_4$)-type crystal structure with unit-cell dimensions of $a = 6.917$ Å and $c = 6.053$ Å. The pure material orders antiferromagnetically at 3.39 K. The lowest Dy^{3+} state is a Kramers doublet of almost pure $|J_z\rangle = \pm 15/2$ character with the first excited state about 120 K above the ground state. The crystalline electric field produces a highly anisotropic Zeeman interaction in the ground-state doublet.

The Hamiltonian representing the Zeeman interaction between an external field $\underset{\sim}{B}$ and the ionic magnetic moment, $\underset{\sim}{\mu} = \beta g_J \underset{\sim}{J}$ is

$$H_{Zeeman} = \beta\, g_J\, \underset{\sim}{B} \cdot \underset{\sim}{J} \quad , \tag{1}$$

where β is the Bohr magneton, g_J is the Lande g-factor, and $\underset{\sim}{J}$ is the total electronic angular-momentum operator. With pure Russell-Sanders coupling, $g_J = 4/3$ for the $^6H_{15/2}$ term of Dy^{3+}. For an isolated Kramers doublet, Eq. (1) may be written in the effective spin S = 1/2 formalism

$$H_{Zeeman} = \underset{\approx}{g}\, \beta\, \underset{\sim}{B} \cdot \underset{\sim}{S} \quad , \tag{2}$$

where $\underset{\approx}{g}$ is now a tensor. The magnetic properties of the ion, including anisotropy, are contained in the g-tensor, which has the following components in a principal-axis system

$$g_{\parallel} = 2g_J \langle \Gamma_1^+ | J_z | \Gamma_1^+ \rangle$$

$$g_{\perp} = 2g_J \langle \Gamma_1^+ | J_{x,y} | \Gamma_1^- \rangle , \tag{3}$$

where $|\Gamma_1^+\rangle$ and $|\Gamma_1^-\rangle$ are symbols for eigenfunctions of the ground doublet. The experimental value of $g_{\parallel}$ (along the tetragonal c-axis) is 19.32 with $g_{\perp} = 0.3 \pm 0.1$ (Ref. 4).

As the crystal rotates in a constant magnetic field, the Zeeman splitting will vary as $\cos\theta$ (θ is the angle between $\underset{\sim}{B}$ and the c-axis) modulated by the g-tensor. The magnetic entropy changes that occur as the crystal rotates are shown in Fig. 1. The curves in Fig. 1 were calculated for the crystal-field plus Zeeman interaction. The Hamiltonian can be written as

$$H = g_J\, \beta\, \underset{\sim}{B} \cdot \underset{\sim}{J} + B_{20} T_{20}(\underset{\sim}{J}) + B_{40} T_{40}(\underset{\sim}{J})$$

$$+ B_{60} T_{60}(\underset{\sim}{J}) + B_{44} \left[T_{44}(\underset{\sim}{J}) + T_{4-4}(\underset{\sim}{J}) \right]$$

$$+ B_{64} \left[T_{64}(\underset{\sim}{J}) + T_{6-4}(\underset{\sim}{J}) \right] \quad , \tag{4}$$

where B_{20}, B_{40}, etc., are the crystal-field splitting parameters and T_{20}, T_{40}, etc., are tensor operators that describe the tetragonal crystal field.[6] The crystal-field parameters for $DyPO_4$ are reported in Ref. 4, but two of the parameters in Table I of Ref. 4 have incorrect values. The values used for the calculations of Fig. 1 are: $B_{20} = -3.391960$ K, $B_{40} = -7.1184281 \times 10^{-3}$ K, $B_{44} = 1.6387877 \times 10^{-1}$ K, $B_{60} = -4.0017428 \times 10^{-3}$ K, and $B_{64} = -7.7915092 \times 10^{-4}$ K. The angle between the c-axis of the crystal and the magnetic field was varied from 0° to 90° in the plane formed by the c- and a-axes.

If the heat of magnetization is removed by exchange fluid at some high temperature, e.g., 20 K, the crystal will cool when it is rotated such that the c-axis is perpendicular to $\underset{\sim}{B}$. If another stream of heat-exchange fluid flows by the crystal when it reaches a specified lower temperature, e.g., 4.2 K, a constant lower temperature will result as heat is transferred from the 4.2 K source to the crystal. If the crystal is then further rotated without any exchange fluid, it will warm to 20 K and the cycle is ready to be repeated. The cycle is a Carnot cycle and is also shown in Fig. 1. The angles required for the different stages can be read from the curves and are summarized in Fig. 2. Hot heat-exchange fluid must be in contact with the crystals between ~115° and 180° and ~295° and 360° (0°); cold heat-exchange fluid must be in contact with the crystals between ~80° and 90° and ~260° and 270°. Note that each segment of the wheel executes the Carnot cycle twice during each revolution.

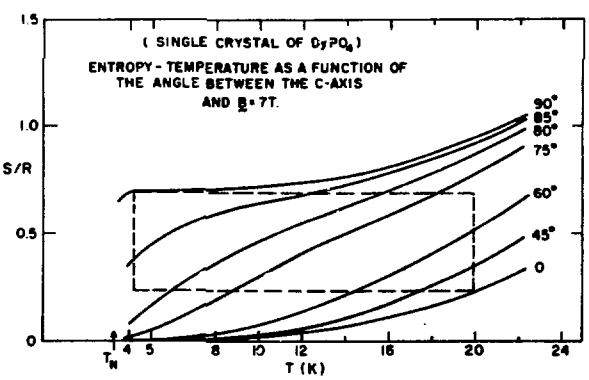

Fig. 1.
Entropy-temperature curves of $DyPO_4$ single crystals as a function of θ, the angle between the c-axis of the crystal and $\underset{\sim}{B}$, the magnetic field. Dashed line shows the Carnot cycle used for the refrigerator calculations.

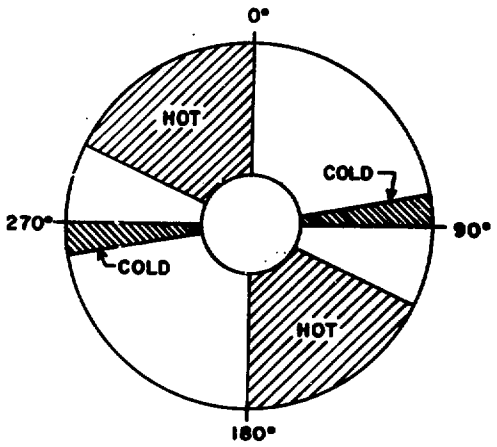

Fig. 2.
Plot of the wheel areas available for the flow of hot and cold helium exchange gas. The plot was derived from the cycle illustrated in Fig. 1.

B. Design Calculations

1. Cooling Power. The cooling power for a rotational refrigerator operating in a Carnot cycle is given by

$$\dot{Q}_C = T_C \, \Delta S \, 2\nu \ , \tag{5}$$

where T_c is the refrigeration temperature, ΔS is the entropy change at that temperature, and ν is the rotation frequency. The factor of 2 is required to account for the double execution of the cycle during each revolution and the resultant doubling of the cooling power. If ΔS is taken as 0.4 R (which is conservative according to Fig. 1), T_c as 4.2 K, with the molar volume of 49.5 cm³/mol (Ref. 5), then

$$\dot{Q}_C = 5.64 \times 10^{-1} \, \nu \ \mathrm{W/cm^3 \ DyPO_4} \ . \tag{6}$$

The rate of heat rejection at 20 K will be given by

$$\dot{Q}_H = T_H \, (\Delta \dot{S}_{IRR} + \dot{Q}_C/T_C) \ , \tag{7}$$

where T_H is the rejection temperature and $\Delta \dot{S}_{IRR}$ is the rate of irreversible entropy created in the cycle. At this stage of the calculation a reasonable estimate of $\Delta \dot{S}_{IRR}$ is ~10% of $\dot{Q}_c/T_c$ and, if T_H = 20 K,

$$\dot{Q}_H = 2.95 \ \nu \ \mathrm{W/cm^3 \ DyPO_4} \ . \tag{8}$$

2. Helium Gas Flow Required to Provide Heat Transfer. To avoid any internal thermal load caused by entrainment, helium gas at 1-atm pressure is used as the heat-transfer fluid. If the cold-bath temperature is always kept slightly higher than 4.2 K, no condensation will occur and no large latent-heat load will occur. The mass flow rate of the helium near 20 K is given by

$$\dot{m}_H = \dot{Q}_H/C_p \, \Delta T \ , \tag{9}$$

where $\dot{m}_H$ is the mass flow rate through the 20 K crystals, C_p is the heat capacity of helium gas at constant pressure, and ΔT is the temperature difference between the input helium gas and the exit helium gas (before and after passing through the $DyPO_4$ crystals). If we take ΔT as ~10% of the reservoir temperature,* C_p = 5.2 J/g·K at 20 K, and C_p = 9.7 J/g·K at 4.2 K (Ref. 8), and $\dot{Q}_H$ from Eq. (8), then

$$\dot{m}_H = 2.84 \times 10^{-1} \, \nu \ \mathrm{g/s} \ . \tag{10}$$

The corresponding cold-bath mass flow rate is

$$\dot{m}_C = 1.38 \times 10^{-1} \, \nu \ \mathrm{g/s} \ . \tag{11}$$

These mass flow rates convert to the following volume flow rates:

$$\dot{V}_H = 1.16 \times 10^{2} \ \nu \ \mathrm{cm^3/s} .$$

$$\dot{V}_C = 8.20 \ \nu \ \mathrm{cm^3/s} \ . \tag{12}$$

3. Wheel Size. The volume of $DyPO_4$ required for a certain cooling power can be obtained from Eq. (6) once a frequency is chosen. However, in the design presented here, the volume of the magnet was chosen to be as small as possible, so the inside diameter of the magnet dictated the wheel diameter

*If heat flows across a temperature gradient ΔT at rate $d\dot{Q}$ with an average temperature T, then the rate of entropy creation is approximately $d\dot{S} = d\dot{Q}\Delta T/T^2$, which for the ~10% ΔT at 20 K gives $d\dot{S} = 6.7 \times 10^{-2}$ W/K/cm³ $DyPO_4$. Such a small entropy creation rate is insignificant compared to the cold-bath entropy change, $\dot{Q}_c/T_c = 1.34 \times 10^{-1}$ W/K/cm³ $DyPO_4$.

of ~2.5 cm. If the porosity of the crystals is 75%, the volume of the wheel will be 4 cm^3 for every 1 cm^3 of $DyPO_4$. If the thickness of the wheel is ~1 cm, the 4 cm^3 can be accommodated in a wheel with a 2.5-cm o.d. on a ~0.64-cm shaft. These dimensions may seem arbitrary now but should be established as a practical lower limit as the calculations proceed. The size could easily be increased!

4. Magnet Design. A magnetic field of ~7 T is required for the rotational-cooling magnetic refrigerator. In addition, the crystals must be able to rotate with respect to the axis of the magnet. Of a number of possible configurations, one of the simplest is shown in Fig. 3. The magnet was designed with a current density of 25 000 A/cm^2 and consists of two coils (~3-cm i.d., ~10-cm o.d.) that are axially separated by a ~1-cm spacer. The spacer provides access for the drive shaft and hot and cold gas ducts. The magnetic-field volume of this magnet is a small fraction of the total magnet volume. Unfortunately, the scaling laws for optimum-size magnets (which use 25 000 A/cm^2 to produce 7 T) do not allow much reduction in the size of the magnet.[8] However, if state-of-the-art magnets with ~50 000 A/cm^2 are made, the magnet volume then will decrease to 100-200 cm^3 for the same field volume. The rotational-cooling refrigerator size is dominated by the magnet size at very low cooling powers. As the cooling-power requirements increase, the ratio of the magnetic-field volume to total magnet volume increases rapidly. Table I shows the ratio of field volume to total magnet volume for optimized 7-T magnets having different inner diameters and using 25 000 A/cm^2 current density.

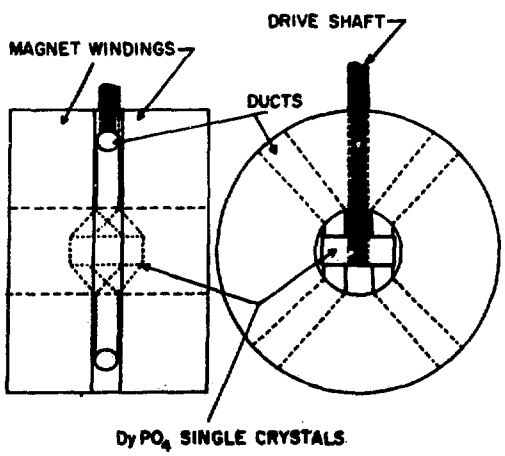

Fig. 3.
Side and end schematics of the wheel of $DyPO_4$ single crystals inside a 7-T magnet.

5. Orifice Pressure Drop. The helium gas must be forced through the small ducts leading into the $DyPO_4$ wheel. The kinetic energy of the gas will increase as the gas flows through the smaller orifice. The additional kinetic energy is later dissipated and produces an orifice pressure-drop loss.

If the orifice area is several times smaller than the duct leading to the orifice, the pressure drop through the orifice can be calculated from

$$dP = 1/2\ \rho \left(\frac{\dot{V}}{A_o}\right)^2 K \ , \qquad (13)$$

where ρ is the helium density, $\dot{V}$ is the volume flow rate, A_o is the orifice area, and K is a constant related to the discharge coefficient; K has a value of ~2 (Ref. 9). On the high-temperature side of the wheel the pressure drop through the ~0.6-cm^2 orifice will be

$$dP_H = 91\ v^2\ dyn/cm^2 = 9.1\ v^2\ Pa \ . \qquad (14)$$

TABLE I

RATIO OF MAGNETIC-FIELD VOLUME TO TOTAL MAGNET VOLUME

Inside Diameter (cm)	Vol. Field/Vol. Magnet for 7 T (%)
1	2.1
2	5.2
3	9.6
4	13.0
4.45	14.9
8.9	27.0
22.3	47.6

The corresponding loss is given by

$$\dot{V}_H dP_H = 1.1 \times 10^{-3} \nu^3 W . \quad (15)$$

Equation (15) shows that the orifice loss is completely negligible at 1 Hz and becomes comparable to the cooling power at ~10 Hz. Only one orifice has been considered, so a factor of 2 may have to be added into the calculation.

6. Pressure Drop Through $DyPO_4$ Crystals. If we assume that the crystals can be fabricated into a porous bed with an effective particle diameter of ~0.5 mm, we can calculate the pressure drop through the bed. The assumption of a 0.5-mm effective particle diameter is not unreasonable, as will be described in the next section. The pressure drop through a porous bed is proportional to the kinetic energy of the fluid in the channels of the bed. The calculation can be done using

$$dP = 1/2\, \rho v^2 \left(\frac{L}{R_H}\right) f , \quad (16)$$

where v is the fluid velocity in the channels of the bed, L is the length of the bed, R_H is the hydraulic radius of the channels in the bed, and f is the friction factor.[9] The friction factor for the whole range of Reynolds numbers can be described by[10]

$$f = 1.75 + 150/Re . \quad (17)$$

Equation (17) is a best estimate made from the data of several workers. The equation for the Reynolds number for porous beds is

$$R_e = \frac{4 R_H \dot{m}}{\mu A_{cs} \alpha} , \quad (18)$$

where A_{cs} is a fraction of the frontal, cross-sectional area of bed (see Fig. 2), α is the porosity, μ is the viscosity of the fluid, and the other terms are as previously defined.[11] The hydraulic radius of a porous-bed channel is calculated by

$$R_H = \frac{\alpha L A_{cs}}{A'} , \quad (19)$$

where A' is the surface area of the crystals in the bed. A' can be calculated using

$$A' = \frac{6(1-\alpha)V_{cont}}{d_p} . \quad (20)$$

If we take $\alpha = 0.75$, as assumed in Sec. II-B-3, then $A' = 120$ cm² for the whole bed of dimensions as given in Sec. II-B-3. Using Fig. 2, we can calculate that the cold fluid has $A' = 8.4$ cm² and the hot fluid has $A' = 43$ cm². Now using Eq. (19), we obtain $R_H = 2.50 \times 10^{-2}$ cm. This result can be substituted into Eq. (18) to give a Reynolds number of 734 on the hot side of the wheel and 3630 on the cold side of the wheel. The first of these Reynolds numbers indicates laminar flow of the 20 K helium gas through the $DyPO_4$ crystals and turbulent flow of the 4 K helium gas through the $DyPO_4$ crystals. If we substitute the superficial velocity, $v_{sf} = v/\alpha$, into Eq. (16), we obtain the following expression for the loss:

$$\dot{V} dP = \frac{\dot{V}^3 \rho L f}{2 A_{cs}^2 \alpha^2 R_H} . \quad (21)$$

The flow losses for the hot and cold segments of the wheel can now be calculated. The results for the hot segments are

$$\dot{V}_H dP_H = 1.27 \times 10^{-2} \nu^3 W , \quad (22)$$

where the exponent of ν is weakly dependent on 1/Re, thus slightly reducing the exponent from 3. The cold segments give

$$\dot{V}_c dP_c = 8.86 \times 10^{-4} \nu^3 W . \quad (23)$$

The results of Eqs. (22) and (23) show that the pressure-drop losses through the $DyPO_4$ crystals are not significant at 1 Hz but would become significant at ~5 Hz.

7. Heat Transfer in the Porous $DyPO_4$ Wheel. A correlation for porous-bed heat transfer by Eckart and Drake[12] gives the following equation for the conductance h:

$$h = \frac{k}{d_p} 0.80 (Re)^{0.7} (Pr)^{0.33} , \quad (24)$$

where k is the thermal conductivity of the helium gas and Pr is the Prandtl number. In this correlation, the Reynolds number is defined as $Re = \dot{m}d_p/\mu A_{cs}$. If the numbers for helium gas are substituted into Eq. (24) and the cold and hot contact areas are used, then

$$h_C A'_C = 6.86\ v^{0.7}\ W/K \qquad (25a)$$

and

$$h_H A'_C = 12.0\ v^{0.7}\ W/K\ . \qquad (25b)$$

This correlation may overestimate the conductance by a factor of 2 but should be approximately correct. If Eqs. (6) and (8) are divided into Eqs. (25a) and (25b), respectively, then $\Delta T_C = 8.2 \times 10^{-2}\ \nu^{0.3}$ K and $\Delta T_H = 0.25\ \nu^{0.3}$ K. The original assumption in Sec. II-B-2 of the design calculations was that ΔT was large enough to give $\Delta S_{IRR} \sim 10\%$ of ΔS. This infers that ΔT is 10-20% of T. Such a large ΔT between the $DyPO_4$ and the helium gas should be more than adequate for heat transfer at low frequencies. The heat-transfer calculations indicate that an operating frequency of several Hertz is possible (for 1 cm^3 of $DyPO_4$, rotation at 10 Hz gives 5 W of refrigeration at 4.2 K).

Another point should be made about the thermal conductivity of the $DyPO_4$ crystal bed. The crystals must be <0.5 mm in diameter because the bulk thermal conductivity of paramagnetic salts is so poor.[18]

III. DISCUSSION

High reliability is an important requirement for airborne and space refrigerators. Magnetic refrigerators have the potential for high reliability because only a few slow-moving parts are required.

The wheel-type magnetic refrigerator[14] has a simple axial drive but a complicated magnetic-field profile problem, at least for low-power systems where the top of a small wheel needs high fields and the bottom needs low fields.[5,15] One solution to the magnetic-field profile problem is to use a wheel that rotates (with a rim drive) through a solenoidal magnet.[16] The latter wheel design has a more complicated drive and requires that the wheel rotate out of the magnet during part of the cycle.

The use of reciprocating magnetic refrigerators at low temperatures is also possible.[17,18] The key problem with that design is the mixing of fluid across a temperature gradient in the regenerator. Disadvantages also include the relatively large size of the refrigerator and the complicated system of two moving parts (magnet and magnetic material, magnetic material and regenerator fluid, magnet and regenerator fluid, or magnet plus displacer).

The rotational-cooling magnetic-refrigerator design minimizes most of these problems. It has only one simple rotary motion. It operates on a Carnot cycle and avoids the complexity of regeneration. The rotational-cooling magnetic refrigerator avoids any field-profile problems because the magnetic anisotropy of the crystal allows operation inside a solenoidal magnet. The scaling laws on magnets do not allow miniaturization of any type of magnetic refrigerator but the rotational-cooling type will be smaller than the wheel or reciprocating type because the working material is enclosed in the magnet during the entire cycle. A lower limit on volume is ~100-200 cm^3 for 7-T magnets.

The major difficulty with the idea of a rotational-cooling refrigerator is the fabrication of the $DyPO_4$ crystals into a porous wheel. Fortunately, $DyPO_4$ single crystals can be readily grown by the molten flux method.[19] The crystals produced are needle-shaped with dimensions of approximately 0.3 × 1 × 4 mm (Ref. 20). These dimensions are excellent for the heat-transfer requirements because the smallest dimension, 0.3 mm, is less than the 0.5 mm used in the calculations. Also fortunate is the fact that the long (4-mm) axis is also the c-, or optic, axis that must rotate about the magnetic-field axis. Several of the 4-mm lengths might be placed end to end such that the 0.3-mm axis was perpendicular to the helium-flow direction. The wheel would have to be radially segmented to avoid transverse flow around the wheel.

The seals to the wheel could be of a labyrinth type because the pressure drops across the 75% porous wheel are extremely small. The ends of the magnet could also be sealed if necessary.

Consider a persistent-mode magnet (with both ends sealed) immersed in a liquid-helium bath. The

ducts could be insulated from the bath and could go to remote sink and source locations. Some of the refrigeration could be used to maintain the bath temperature indefinitely. The drive-shaft seal could be brought above the liquid level and could be a simple labyrinth seal. The spacer of the magnet that separates the two coils would have to be made of strong material of poor thermal conductivity to avoid thermal short-circuiting of the 4.2 K and 20 K helium-gas ducts.

The efficiency of the magnetic refrigerator over the 4 K to 20 K range will be high because the magnetic entropy changes are large and reversible. The major irreversible entropy creation comes from the heat transfer. For 1-mW to 1-W operation, the temperature gradients for heat transfer should be $\ll$10% of the operating temperatures. Such a small temperature gradient will yield high efficiency. The rotational-cooling refrigerator should have 70-90% of Carnot efficiency.

The cooling power can be varied by simply varying the rotation rate. The exact rotation rate required for various powers will depend on the residual losses. One watt of cooling power should be obtained at ~2 Hz.

Materials other than $DyPO_4$ are suitable for rotational cooling. Several examples, discussed in the Appendix, illustrate the desirability of a further search for additional magnetic systems having the required anisotropic properties.

APPENDIX

Several crystalline systems, such as $DyPO_4$, exhibit anisotropic magnetic properties. Generally, these systems have a doublet ground state with an excited state at $\gtrsim$100 K. Therefore, the maximum entropy that can be used in a cycle to low temperatures is R ℓn 2. A rotational-cooling refrigerator would be even more attractive if we could find materials that had more entropy available at low temperatures. Such systems would generally be metallic, rare-earth alloys having a smaller crystal-field splitting than many of the crystalline compounds like $DyPO_4$. The entropy change in three rare-earth systems (Figs. A-1, -2, and -3) has been calculated as a function of the angle between the magnetic-field and the fourfold cubic axis of the crystal. The crystal-field-interaction data were taken from Refs. 21-23. None of these three samples is especially suitable for 4 K to 20 K operation without regeneration, but each could operate over a reduced temperature span, particularly with regeneration. The three examples were chosen on the basis of prior experience, but a serious investigation might uncover many other superior systems.

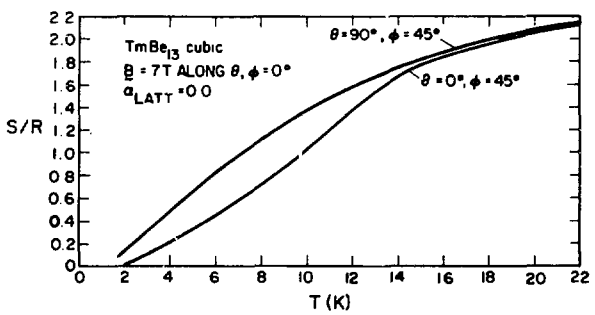

Fig. A-1.
Entropy-temperature curves of $TmBe_{13}$ single crystals as a function of θ, the angle between the fourfold cubic axis of the crystal and B, the magnetic field.

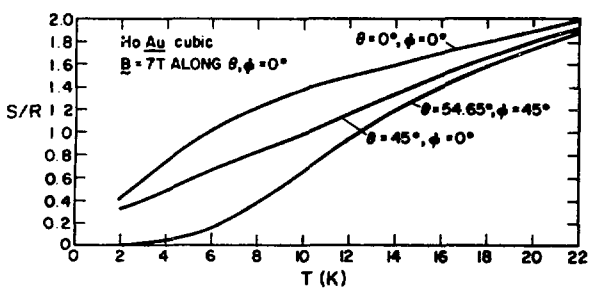

Fig. A-2.
Entropy-temperature curves of HoAu single crystals as a function of θ, the angle between the fourfold cubic axis of the crystal and B, the magnetic field.

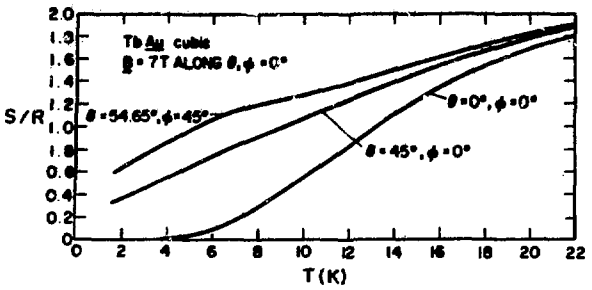

Fig. A-3.
Entropy-temperature curves of $TbAl_2$ single crystals as a function of θ, the angle between the fourfold cubic axis of the crystal and B, the magnetic field.

REFERENCES

1. C. D. Jeffries, "A Proposal for Nuclear Spin Cooling," Cryogenics **3**, 41 (1963).

2. A. Abragam, "Some New Schemes for Dynamic Nuclear Polarization," Cryogenics **3**, 42 (1963).

3. J. Button-Shafer, R. L. Lichti, and W. H. Potter, "High Proton Polarization Achieved with a $(Yb,Y)(C_2H_8SO_4)_3 \cdot 9\ H_2O$ Spin Refrigerator," Phys. Rev. Lett. **39**, 677 (1977) and references therein.

4. D. W. Forester and W. A. Ferrando, "Mössbauer Study of $DyPO_4$: Hyperfine Parameters, g-Factor Anisotropy, and Spin-Lattice Relaxation," Phys. Rev. **13B**, 3991 (1976).

5. W. P. Pratt, Jr., S. S. Rosenblum, W. A. Steyert, and J. A. Barclay, "A Continuous Demagnetization Refrigerator Operating near 2 K and a Study of Magnetic Refrigerants," Cryogenics **17**, 689 (1977).

6. H. A. Buckmaster and Y. H. Shing, "A Survey of the EPR Spectra of Gd^{3+} in Single Crystals," Phys. Status Solidi **A12**, 325 (1972).

7. R. D. McCarty, "Thermophysical Properties of Helium-4 from 2 to 1500 K with Pressures to 1000 Atmospheres," National Bureau of Standards report NBS-TN-631 (1972).

8. E. J. Thomas and C. D. Bright, "Optimizing the Design of Superconducting Solenoids," Cryogenics **6**, 10 (1966).

9. R. Bird, W. Stewart, and E. Lightfoot, *Transport Phenomena* (John Wiley and Sons, New York, 1960), Chap 6.

10. W. A. Steyert and N. J. Stone, "Low Flow Velocity, Fine-Screen Heat Exchangers and Vapor-Cooled Cryogenic Current Leads," Los Alamos Scientific Laboratory report LA-7395 (September 1978).

11. J. E. Coppage and A. L. London, "Heat Transfer and Flow Friction Characteristics of Porous Media," Chem. Eng. Prog. **52**, 57 (1956).

12. E. R. G. Eckert and R. M. Drake, Jr., *Heat and Mass Transfer* (McGraw-Hill, New York, 1959).

13. J. A. Barclay, L. Paterson, D. Bingham, and O. Moze, "Low Temperature Conductivity of $Gd_2(SO_4)_3 \cdot 8\ H_2O$ and $Dy_2Ti_2O_7$ as a Function of Magnetic Field," Cryogenics **18**, 535 (1978).

14. W. A. Steyert, "Rotating Carnot Cycle Magnetic Refrigerators for Use near 2 K," J. Appl. Phys. **49**, 1227 (1978).

15. J. A. Barclay and W. A. Steyert, "Magnetic Refrigerator Development," Los Alamos Scientific Laboratory report LA-7913-PR (October 1979).

16. J. A. Barclay and W. A. Steyert, "Magnetic Refrigerator for Space Applications," Los Alamos Scientific Laboratory report LA-8134, to be published.

17. J. R. Van Geuns, "A Study of a New Magnetic Refrigerating Cycle," Philips Res. Rep. Suppl. No. 6 (1966) (Eindhoven, Netherlands).

18. J. A. Barclay, O. Moze, and L. Paterson, "A Reciprocating Magnetic Refrigerator for 2-4 K Operation: Initial Results," J. Appl. Phys. 50, 5870 (1979).

19. R. S. Feigelson, "Synthesis and Single-Crystal Growth of Rare-Earth Orthophosphates," J. Am. Ceram. Soc. 47, 257 (1964).

20. J. C. Wright, H. W. Moos, J. H. Colwell, B. W. Mangum, and D. D. Thornton, "$DyPO_4$: A Three-Dimensional Ising Antiferromagnet," Phys. Rev. B3, 843 (1971).

21. E. Bucher, J. P. Maita, G. W. Hull, R. C. Fulton, and A. S. Cooper, "Electronic Properties of Beryllides of the Rare Earths and Some Actinides," Phys. Rev. 11B, 440 (1975).

22. A. P. Murani," Magnetic Susceptibility and Electrical Resistivity of Some Gold-Rare Earth Alloys," J. Phys. C Suppl. 2, 5153 (1970).

23. J. A. Barclay and B. Perczuk, "Crystal Field Measurement for Tb^{3+} in Gold," Solid State Commun. 17, 565 (1975).